Physica Medica 63 (2019) 48–55

Contents lists available at ScienceDirect

Physica Medica

journal homepage: www.elsevier.com/locate/ejmp

Original paper

Quality evaluation of monoenergetic images generated by dual-energy computed tomography for radiotherapy: A phantom study

Bartosz Pawałowski[a,b], Hubert Szweda[a], Alina Dudkowiak[b], Tomasz Piotrowski[a,c,*]

[a] Department of Medical Physics, Greater Poland Cancer Centre, Poznań, Poland
[b] Department of Technical Physics, Poznan University of Technology, Poznan, Poland
[c] Department of Electroradiology, Poznań University of Medical Sciences, Poznań, Poland

ARTICLE INFO

Keywords:
Spectral CT
Monoenergetic CT
Dual energy
Quality of CT images

ABSTRACT

Purpose: Quantification analysis for monoenergetic computed tomography (CT) images obtained from dual-energy CT scanning was performed in the light of their potential use for structures delineation during radiotherapy.

Methods: Parameters that describe the quality of the images are: linearity, low and high contrast resolution, uniformity, noise and signal to noise ratio (SNR). To evaluate these parameters, a Catphan phantom was scanned using a dual-energy mode at Somatom Definition AS. Based on the polyenergetic CT images, sixteen monoenergetic series (ranged from 40 keV to 190 keV) were created by CT scanner software and automatically analyzed using Artiscan software.

Results: Analysis of linearity shows that a potential use of any monoenergetic images in radiotherapy planning requires that individual calibration curves are implemented for each of them. While the results of the high contrast resolution analysis were comparable for each energy (5 lp/cm), the results of the analyses for uniformity, low contrast resolution, noise and SNR allowed us to select the best imaging energies. The highest relative uniformity was detected for images reconstructed for energies of 60 keV and 70 keV (98.54% and 98.61%). Similar results were observed for low contrast resolution, where the largest number of disks was detected for these energies, and the noise values (0.42% for 60 keV, 0.44% for 70 keV). The best SNR was observed for images reconstructed for energy of 60 keV.

Conclusions: Taking into account these results, the energy of 70 keV was selected as potentially the best for reconstruction of monoenergetic images used for structures delineation during radiotherapy.

1. Introduction

Limited differentiation of anatomical structures on computed tomographic (CT) images significantly affects the precision of the determination of the target volumes and organs at risk during the segmentation process which is one of the crucial parts of the treatment planning procedure performed before radiation therapy [1,2]. In the case of dynamic techniques of radiation therapy (e.g. intensity modulated radiation therapy or volumetric modulated arc therapy), inaccuracy of segmentation affects directly the optimization of dose distribution during the treatment plan preparation and, eventually, the accuracy of dose deposition during the treatment. The reason for these difficulties is that the CT-numbers measured for a specific voxel (representing an elemental part of the tissue) is related to the linear attenuation coefficient μ(E) which is not unique for any given tissue/material, but is a function of the material composition, the photon energies interacting with the material, and the mass density of the material [1]. Assuming the use of monoenergetic x-rays, at approximately 120 keV, the same linear attenuation coefficients can be measured for example, for calcified plaques and iodine-containing lymph nodes [1]. Data acquired at approximately 70 keV would allow the differentiation of the two materials.

This was a prerequisite for the development of new computed tomography technologies, which, apart from imaging capabilities using a polyenergetic spectrum of radiation with defined nominal energy, would enable to obtain a few anatomically identical sets of images differentiated by the energy of radiation during one imaging session on CT in such a way that each set of images is related to specific monoenergetic radiation (monoenergetic CT). There are several technical solutions to generate monoenergetic CT images. First group of them is

* Corresponding author at: Department of Medical Physics, Greater Poland Cancer Centre, Garbary 15, 61-866 Poznan, Poland.
E-mail address: tomasz.piotrowski@me.com (T. Piotrowski).

https://doi.org/10.1016/j.ejmp.2019.05.019
Received 27 November 2018; Received in revised form 8 April 2019; Accepted 25 May 2019
Available online 29 May 2019

based on using two or more polyenergetic spectrums with different nominal energies (e.g. 80 keV and 140 keV) and is realized, respectively, by: (i) a system of two x-ray tubes [3–5], (ii) technology of fast switching of scanning energy between possible highest and lowest nominal energy [6–8], or (iii) double helix technique, where the object is scanned twice (each time using a different nominal energy) [9,10]. The second group of technical solutions applies to the construction of CT detectors, e.g. (i) two-layer detectors, where the surface layer collects a signal with lower energies and the layer located deeper collects a signal with higher energies [11–14], or (ii) technology based on counting single photons for which the detector is a semiconductor diode that allows to detect single photons and correlate the strength of the detected signal with energy [15–18].

Use of a different set of monoenergetic images based on the spectral analysis allows to resolve problems with non-differentiated structures for conventional imaging (polyenergetic CT with specified nominal energy of radiation). When the anatomical data are non-contrasted and free of high-density material, there is a possibility to select the monoenergetic set of images that, based on the parameters characterizing the image quality, are most appropriate for treatment plan preparation.

2. Material and methods

The aim of this study was to evaluate the monoenergetic CT images collected by the dual-energy mode using the double helix technique on the Somatom Definition AS machine (Siemens Medical Solutions, Erlangen, Germany). The evaluation was performed on the images gathered for the Catphan 504 (CTP504) phantom (The Phantom Laboratory, Salem, NY, USA). The CTP504 was placed on the CT table in such a way that only the basis of the phantom was on the table while the active (imaged) part of the phantom was outside the table during scanning (Fig. 1a). The slice thickness of 3 mm, 1.2 value of the pitch and 80 keV and 140 keV energies for the first and the other helix, respectively, were used during imaging of the phantom. The CT dose volume indices ($CTDI_{vol}$) and dose length products (DLP) were, respectively: 16.8 mGy and 369.6 mGy*cm for the first helix (80 keV); and 18.4 mGy and 404.8 mGy*cm for the other helix (140 keV). Based on the obtained set of dual-energy CT images, the reconstructions of the sixteen monoenergetic CT sets of images were performed with energies ranging from 40 keV to 190 keV with a step of 10 keV. Fig. 1b shows the operation window available in the reconstruction module of software installed on an operator station of the Somatom Definition AS machine, where a monoenergetic CT set of images is created from the dual-energy CT set of images. The energy selection slider located at the bottom of the window on Fig. 1b allows to extract the monoenergetic data ranged from 40 keV to 140 keV from data gathered during scanning and extrapolate these data to the monoenergetic data for energies from 141 keV up to 190 keV.

All quantitative analyses of the quality of images included in this study were performed in the Artiscan software (AQUILAB, Loos les Lille, France) enabling automatic analysis of the CT images gathered for the CTP504 phantom. The CTP504 is 20 cm in length and includes four modules dedicated for measurements of the parameters of CT images describing their quality [19,20]. For each monoenergetic CT set of images, the following parameters were evaluated: (i) linearity of the CT-numbers for different mass densities displayed on different monoenergetic CT sets of images (imaging data collected in CTP401 module), (ii) low contrast resolution (imaging data collected in CTP515 module), (iii) uniformity, noise and signal to noise ratio (imaging data collected in CTP486 module), and (iv) high contrast resolution (imaging data collected in CTP528 module).

According to the Artiscan brochure describing details of parameters [21] the low contrast resolution, uniformity, noise and signal to noise ratio were expressed, respectively, as:

$$C_o = \frac{S_O - S_F}{S_F} \times 100 \quad (1)$$

where C_O is the low contrast resolution, S_O is the mean signal value collected on the object and S_F is the mean signal value of the signal from the background around the object.

$$Uni = \frac{NdG_{max} - NdG_{min}}{NdG_{max} + NdG_{min}} \quad (2)$$

where Uni is the uniformity, and NdG_{max} and NdG_{min} are, respectively, the maximum and minimum gray levels measured in the region of interest.

$$N = \frac{\sigma_{NH}}{HU_{Water} - HU_{Air}} \times 100\% \quad (3)$$

where N is the noise level, σ_{NH} is the standard deviation of the Hounsfield units in the region of interest, and HU_{Water} and HU_{Air} are, respectively, the Hounsfield units for water and for air.

$$SNR = \sqrt{2}\frac{GL}{\sigma_{Dif}} \quad (4)$$

where SNR is the signal to noise ratio, GL is the mean value of gray

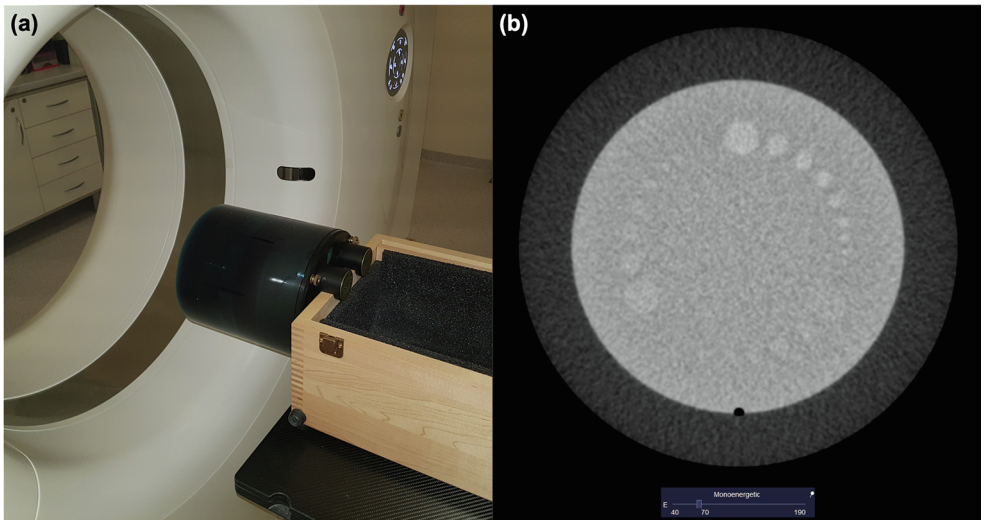

Fig. 1. The Catphan 504 – phantom used in the study. Figures show: (a) position of the phantom during data gathering and (b) image of CTP515 module of the phantom with energy selector at the bottom of the window.

levels in the region of interest and σ_{Dif} is the standard deviation of the gray level difference in the region of interest.

The high contrast resolution was calculated from the ratios for the 21 test patterns of the insert in the phantom (CTP528 module). The power spectral density ratio curve was plotted according to the all test patterns, expressed as pairs of lines per unit of measure. This curve tends towards 100% for the largest pattern and towards 0% when the imaging system can no longer distinguish between them. The first minimum of the curve gives the high contrast resolution. The power spectral density is defined as [21]:

$$PSDR_i = \frac{PSD_{acq}}{PSD_{rec}} \times 100 \quad (5)$$

where $PSDR_i$ is the power spectral density PSD for the *i-th* pattern R_i, and PSD_{rec} and PSD_{acq} are the power spectral densities for the reconstituted theoretical profile and for the acquired profile, respectively.

To analyze the linearity, absolute differences (AD) [HU] and absolute relative differences (ARD) [%] between CT-numbers were measured on monoenergetic and polyenergetic (dual-energy mode) images. The AD and ARD were expressed as follows:

$$AD_{MEj,Di} = |CTnumber_{MEj,Di} - CTnumber_{DE,Di}| \quad (6)$$

$$ARD_{MEj,Di} = \left|\frac{CTnumber_{MEj,Di} - CTnumber_{DE,Di}}{CTnumber_{DE,Di}}\right| \cdot 100\% \quad (7)$$

where $CTnumber_{MEj,Di}$ is an average value of Hounsfield units detected in pixels contained in the *i-th* disc (D_i) at the monoenergetic CT set of images reconstructed for the *j-th* energy (ME_j), $CTnumber_{DE,Di}$ is an average value of Hounsfield units detected in pixels contained in the *i-th* disc (D_i) at the polyenergetic CT set of images obtained from imaging based on the dual energy mode (DE).

3. Results

Based on the linearity analysis, the absolute differences (AD) and absolute relative differences (ARD) between the CT-numbers from monoenergetic and polyenergetic (dual energy mode) CT images were computed. Fig. 2 shows the relations of these values in the light of different relative electron densities displayed on different monoenergetic CT sets of images. The relative electron densities ranged from low values (e.g. 0.001 e/cm^3 for air) through the values comparable to electron densities for water (e.g. 0.998 e/cm^3 for polystyrene) to high values (e.g. 1.868 e/cm^3 for teflon). Based on values of the AD (Fig. 2a) and ARD (Fig. 2b) parameters, the most consistent and the smallest values were observed for energy of 70 keV (1 HU and 0.1% for air, 2HU and 5.9% for polystyrene, and 3HU and 0.3% for teflon). The highest inconsistency was observed for energy of 40 keV: 2 HU and 0.2% for air, 111 HU and 302.1% for polystyrene, and 156 HU and 16.2% for teflon. While the ARD parameter is small for low (air) and high (teflon) relative electron densities, the values of ARD increase for relative electron densities near 1 e/cm^3. For example, for CT images reconstructed for energy of 120 keV the ARD is: 0.4% for air (0.001 e/cm^3), 91.3% for polystyrene (0.998 e/cm^3) and 4.9% for Teflon (1.868 e/cm^3).

Fig. 3 shows the results for low contrast resolution analysis performed in the CTP515 module of CTP504. The CTP515 module contains low contrast supra-slice discs with diameters ranging from 2 mm to 15 mm, and contrast levels of 0.3%, 0.5% and 1.0%. These discs are used to evaluate the ability to differentiate objects with slightly different densities. The first column of the graphical table in Fig. 3 represents the diameters of the discs. The analysis was performed for monoenergetic CT sets of images reconstructed for energies ranging from 40 keV to 190 keV (last row in Fig. 3). The results for contrast levels of 1.0%, 0.5% and 0.3% are presented in the first, second and third column, respectively, for each energy (Fig. 3). While the green dots in Fig. 3 represent the positive result of detection (disc is visible), the red dots mean that no disc was detected. The best results of low contrast resolution analysis were observed for energies of 70 keV and 60 keV. For both of these energies, all discs with contrast level of 1% were visible. For the contrast level of 0.5%, the disc with a diameter of 2 mm, and for the contrast level of 0.3%, discs with diameters of 2 mm, 3 mm and 4 mm were not detected for these energies. The worst results were observed for all energies higher than 120 keV. For these energies, only the discs with diameters higher than 2 mm verified on the contrast

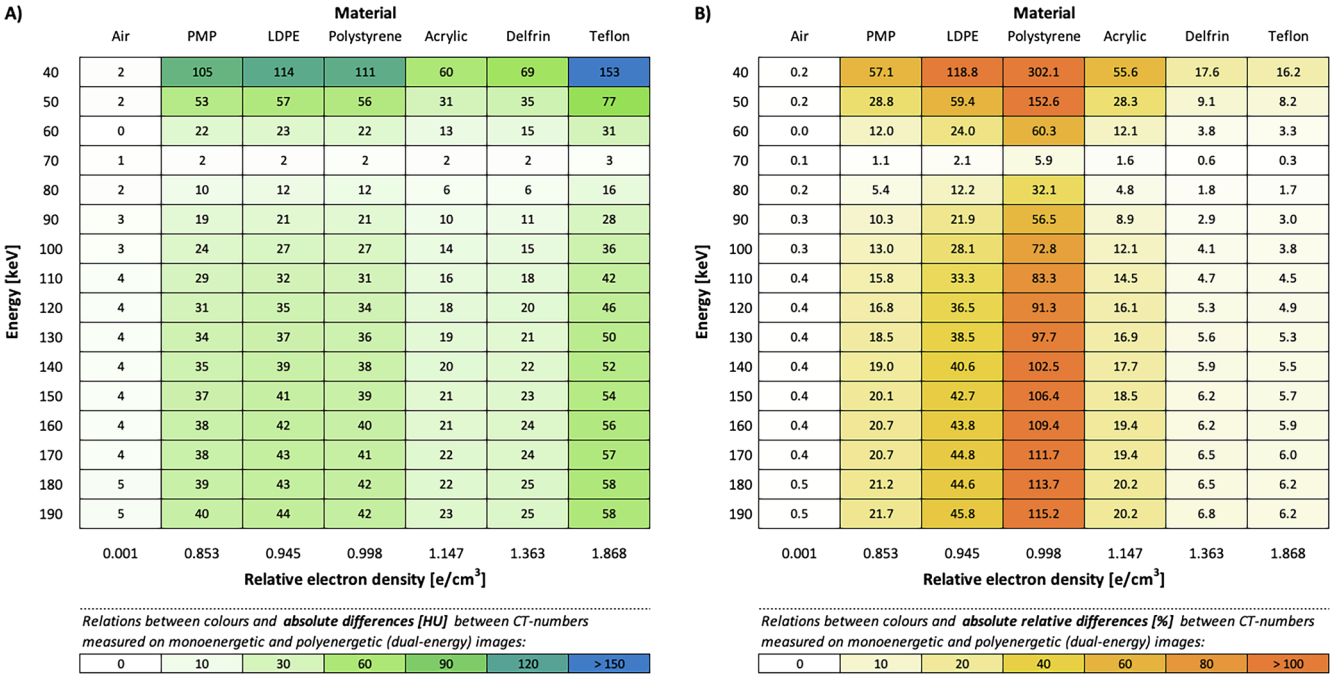

Fig. 2. The absolute differences (a) and the absolute relative differences (b) between the CT-numbers from monoenergetic and polyenergetic (dual energy mode) CT images and their relations to different relative electron densities and different monoenergetic CT sets of images.

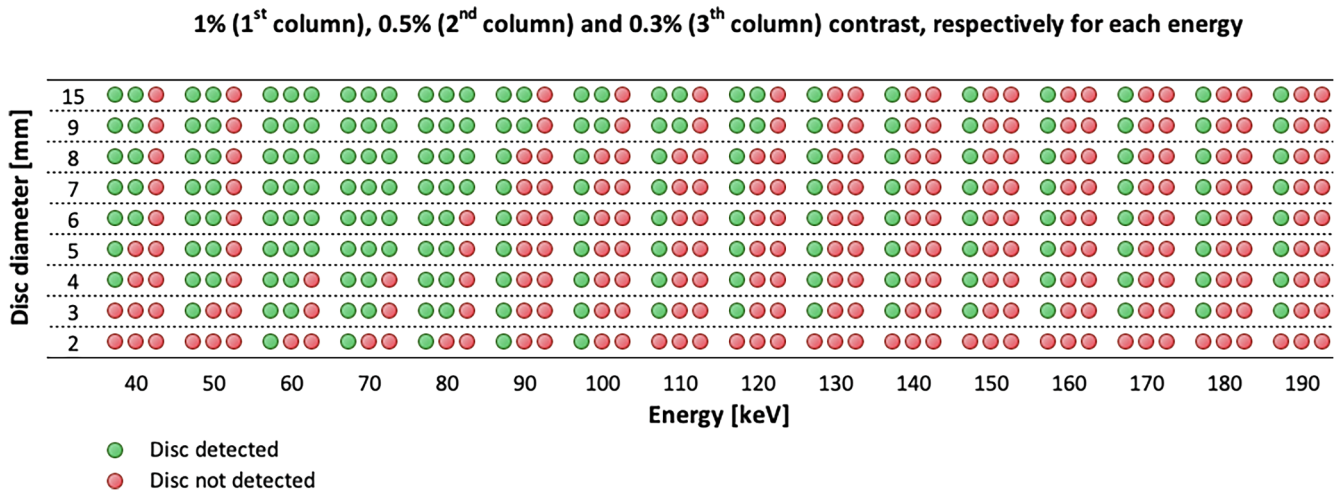

Fig. 3. The results for low contrast resolution analysis performed in the CTP515 module of the Catphan 504 phantom. The green dots represent the positive result of detection, the red dots mean that no disc was detected. (For interpretation of the references to colour in this figure legend, the reader is referred to the web version of this article.)

Table 1
High contrast resolution, relative uniformity, noise and signal to noise ratio in relation to the energies of monoenergetic CT images.

Energy [keV]	High Contrast Resolution [lp/cm]	Relative Uniformity [%]	Signal to Noise Ratio	Noise [%]
40	5.63	92.42	54.66	2.21
50	5.74	96.58	129.00	0.98
60	5.79	98.54	300.00	0.42
70	5.82	98.61	254.90	0.44
80	5.85	98.04	175.81	0.63
90	5.86	97.47	142.45	0.78
100	5.88	97.09	125.67	0.88
110	5.88	96.86	115.72	0.96
120	5.88	96.62	110.01	1.01
130	5.89	96.54	105.51	1.06
140	5.89	96.44	103.20	1.09
150	5.90	96.35	100.35	1.12
160	5.90	96.26	98.74	1.13
170	5.90	96.24	97.49	1.15
180	5.90	96.21	96.51	1.16
190	5.90	96.17	95.68	1.17
Dual-Energy*	5.83	98.66	227.41	0.49

*Images obtained from scanning with two polyenergetic beams with nominal energies of 80 keV and 140 keV (dual energy mode). Data from dual energy mode are the source for reconstruction of monoenergetic images.

level of 1% were detected.

The results of high contrast resolution as well as relative uniformity were presented in Table 1. While almost the whole table contains data for specified energy, the last row of Table 1 contains data for polyenergetic imaging (dual energy mode). Despite a difference between high contrast resolution measured at monoenergetic and polyenergetic CT sets of images, the results are comparable because, in fact, 5 lines pair per cm were detected for every energy.

The best relative uniformity for the monoenergetic CT sets of images was obtained for 70 keV energy (98.61%). The relative uniformity for images obtained from this energy correspond to the relative uniformity for the polyenergetic images (98.66%). For the rest of monoenergetic images, except the images obtained for the energy of 40 keV, the relative uniformity ranged from 96% to 98% and was slightly worse than for the polyenergetic images. The relative uniformity for 40 keV images was significantly worse than for polyenergetic images and was 92.42%.

In addition to the data of high contrast resolution and relative uniformity, Table 1 includes data of noise and signal to noise ratio (SNR) that were visualized in Fig. 4. Among all analyzed energies, the best SNR and the lowest value of the noise were observed for images obtained for the energies of 60 keV and 70 keV.

Moreover, images obtained for these energies were characterised by better values of SNR and noise than the polyenergetic images. The noise and SNR were respectively: 0.42% and 300.00 for 60 keV, 0.44% and 254.90 for 70 keV and 0.49% and 227.41 for polyenergetic images.

4. Discussion

In connection to the technical solutions of the CT scanner used in our hospital (Somatom Definition AS), the evaluation of the monoenergetic CT images was limited to the dual-energy mode realized by the double helix technique. The double helix technique at the Somatom Definition AS scanner consists of two successive spiral scans, where the first scanning uses the energy of 140 keV and the other, the energy of 80 keV. One of the potential limitations of this method is the time delay between the two helixes that can lead to inaccurate imaging of tissues and organs susceptible to motion [1]. In our study, analysis was performed for data gathered from the static phantom. Therefore, the study is free of potential influence of inaccuracy caused by movement. Because our therapeutic line is based on Varian products, the CTP504 was the phantom that was used by us for data gathering [22]. To eliminate the potential influence of the CT table on the images, the CTP504 was placed on the CT table in such a way that the active (imaged) part of the phantom was outside the table during the scanning process (Fig. 1a). To reduce inaccurate image reconstruction at the edges of the active part CTP504 with a full length of 20 cm, a 1 cm margin was used from each side of the phantom. As a result, the scanned length was 22 cm. Therefore, total (for both helixes) $CTDI_{vol}$ and DLP were 35.2 mGy and 774.4 mGy*cm. In contrast to conventional scanning (e.g. when a polyenergetic spectrum of radiation with nominal energy of 120 keV is used), total $CTDI_{vol}$ for the dual energy mode available on our CT scanner is fixed and cannot be modified. This makes it impossible to reduce the dose during scanning. Nevertheless, the total $CTDI_{vol}$ for the dual energy mode is not dramatically higher than every $CTDI_{vol}$ obtained for conventional scanning. For example, in our hospital, for conventional scanning and routinely used protocols, such as protocols for the abdomen and head, the $CTDI_{vol}$ and DLP (for 22 cm) were 14.9 mGy and 327.8 mGy*cm (for abdomen), and 59.4 mGy and 1306.8 mGy*cm (for head). These values were obtained for the same conditions (pitch and slice thickness) as used for dual energy scanning.

The monoenergetic CT images collected by the dual-energy mode were evaluated in the light of parameters characterizing their quality. The quantification analysis of linearity, uniformity, noise and signal to

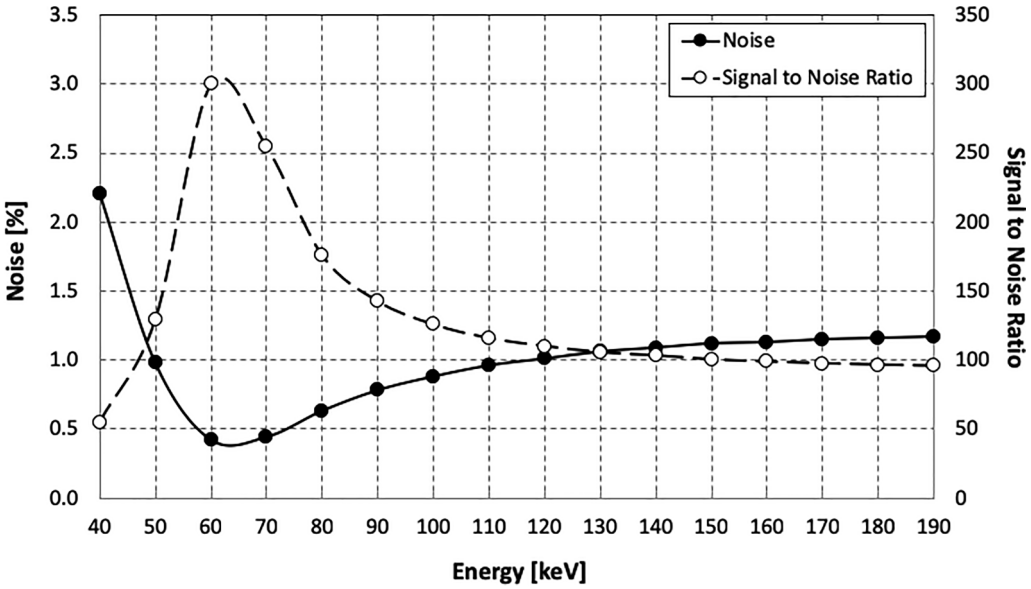

Fig. 4. Noise and signal to noise ratio in relation to the energies of monoenergetic CT images.

noise ratio, and low and high contrast resolution were performed by us with the Artiscan software. The automation tools implemented in the Artiscan software use well-known and widely accepted calculation formalizations. The Artiscan automate manual and objective operations were performed by the investigator for the analysis of linearity, uniformity, noise and signal to noise ratio. The classical assessment of low contrast is based on measurements made by counting numbers of visible targets by the investigator. To maintain reproducibility, the measurements should be carried out by the same investigator and on the same monitor screen with the same viewing conditions (same window settings, same day, subdued ambient light). To minimize all possible factors influencing the results and subjective interpretation of the investigator, Artiscan software performs these measurements automatically. As in low contrast measurements, the classical (visual) evaluation of high resolution is replaced by automated measuring. While automation reduces the impact of inter-observer effect on the obtained results, there is still a question of whether the detection made by the computer is compatible to an average detection performed by investigators in a classical way. Nevertheless, the concept of our study prevents us from addressing this problem because the analysis was based on the evaluation of the parameters computed always in the same way (by Artiscan) between different monoenergetic CT images.

The results from the analysis of linearity (Fig. 2) clearly show that CT-numbers counted for different materials at monoenergetic images differ from one another and are different from CT-numbers counted on polyenergetic images. It means that a potential use of any monoenergetic images in radiation therapy planning, requires that individual calibration curves are implemented for each of them. While individual calibration curves require an absolute difference for evaluation (Fig. 2a), the absolute relative differences (Fig. 2b) show the strength of the absolute differences in the light of the HU ranges detected in structures with specified relative electron density and imaged by different energies. The lowest differences between monoenergetic and polyenergetic images were observed for the energy of 70 keV (Fig. 2). This is caused by the fact that the energy of 70 keV is a main component of the polyenergetic spectrum of radiation used during scanning by the dual energy mode. While the results of a high contrast resolution analysis were comparable for each energy (5 lp/cm), the results of analyses for relative uniformity, low contrast resolution, noise and SNR allowed us to select the best imaging energies. The highest relative uniformity was detected for images reconstructed for energy of 70 keV (98.61%). The best results for low contrast resolution (Fig. 3) and the noise values (Table 1) were observed for energies of 70 keV and 60 keV. Images obtained for both of these energies were characterized by better signal to noise ratios than polyenergetic images (Fig. 4 and Table 1). All the results analyzed and discussed above were gathered in CTP504. Fig. 5 shows images of the head and neck anatomy gathered for monoenergetic (for energies of 50 keV, 70 keV, 120 keV) and mixed (polyenergetic) imaging.

Fig. 5 complement visually the data collected in Table 1. In conjunction to the limitations of the double helix technique, we decided to visualize the head and neck region characterized by relatively low organ flexibility during scanning.

Using one calibration curve (e.g. calibration curve for polyenergetic images) for different sets of monoenergetic images causes inaccuracies of dose calculation. It results directly from the differences in linearity between sets of monoenergetic images (Fig. 2) and their different relative uniformity (Table 1). Fig. 6 shows an example of differences between doses calculated on sets of images differing in energy (50 keV, 70 keV, 120 keV and polyenergetic images) while one calibration curve (for polyenergetic images) was applied. The treatment plans were prepared for Varian TrueBeam™ accelerator (Varian Medical Systems, Palo Alto, CA, USA) using the Eclipse™ treatment planning system ver. 13.6 (Varian Medical Systems, Palo Alto, CA, USA). The analytic anisotropic algorithm with the spatial resolution of 2.5 mm was used for computing dose to the irradiated region. The same simple geometry of the therapeutic beams (i.e. two lateral photon beams with 6 MeV energy, normalised in the same isocentre point) was used for each calculation. As can be seen in Fig. 6, the smallest inaccuracies in the calculation of the dose were observed for images obtained for the energy of 70 keV. This is due to the smallest differences of the linearity and relative uniformity between these images and the polyenergetic images. Nevertheless, it should be clearly noted that the usage of different sets of monoenergetic images during dose calculation induces the need of adding individual calibration curves for each set.

While the linearity and relative uniformity impact the accuracy of the dose calculation, the noise, SNR and low contrast resolution impact the clarity and detail of the images (Fig. 5) that can affect the accuracy of the contouring for specific parts of patient's anatomy. Fig. 7 shows the outlines of bones and the tongue prepared on four different sets of images, i.e. on three monoenergetic sets with energies of 50 keV, 70 keV and 120 keV, and on one set of polyenergetic images.

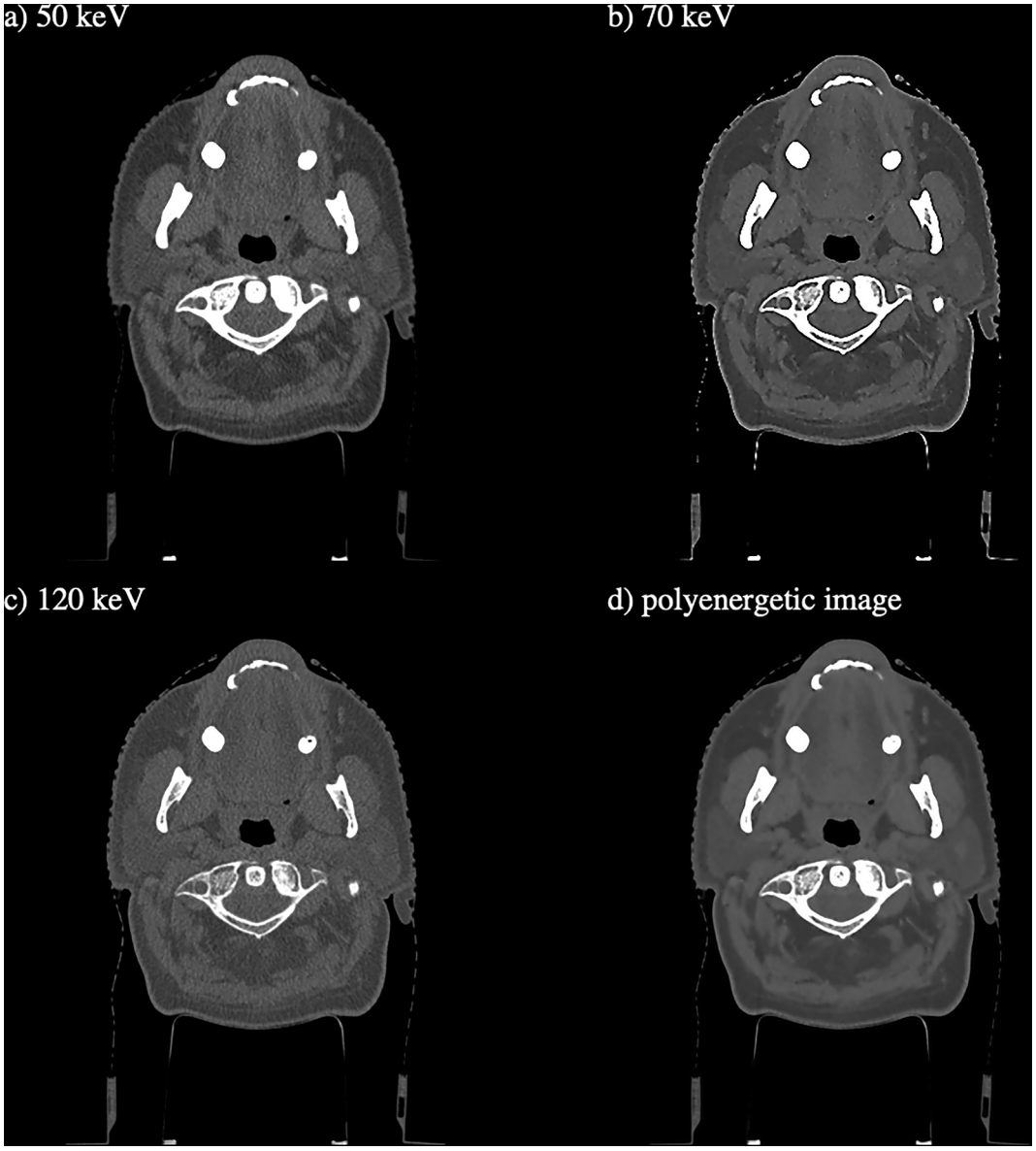

Fig. 5. Head and neck anatomy gathered for (a-c) monoenergetic imaging (respectively: a) 50 keV, b) 70 keV, c) 120 keV), and (d) mixed (polyenergetic) imaging. For each image the same displaying settings were used (window width: 1160 and level: 140).

The bones were outlined automatically, and the tongue was outlined manually by a well experienced radiation oncologist. 70 keV images were indicated by the radiation oncologist as the clearest and most useful during segmentation. Therefore, the outlines performed on this set of images was established as the reference for outlines performed on the other sets of images (50 keV, 120 keV and polyenergetic). Differences between referenced outline and the other outlines were analysed by the Sørensen–Dice coefficient (DSC) [23,24] and by the relative volumes of the outlined structures. The DSC was defined in this example as:

$$DSC = \frac{2(V_R \cap V_X)}{V_R + V_X} \quad (8)$$

where V_R is the volume of structure obtained during segmentation on the set of 70 keV images, V_x is the volume of structure obtained during segmentation on the other sets of images and

$V_R \cap V_X$ is a common part of these volumes.

The relative volumes (V_{norm}) were defined in per cent as the relation between the volume of the structure obtained during segmentation on the other sets of images (V_X) to the volume of structure obtained during segmentation on the set of 70 keV images (V_R).

Table 2 shows the results of analysis for the differences between the reference outline and the other outlines. For both methods of segmentation (automatic for bones and manual for tongue), the differences between the coverage of the outlines performed on different sets of images as well as the differences in relative volumes were detected. These differences can affect the dose distribution in the treatment plans for dynamic techniques of radiotherapy (e.g. intensity modulated radiotherapy or volumetric modulated arc therapy) where inverse planning is used.

Both of these examples are limited to one patient and one investigator (physicist in the first example and radiation oncologist in the other one). Therefore, it should be interpreted as a clinical illustration of our analysis rather than a fundamental part of our study. In future studies, reconstructed monoenergetic scans for 70 keV will be analyzed for clinical use for tumor and organs at risk delineation.

Taking the results of this study, the energy of 70 keV was selected as potentially the best for the reconstruction of monoenergetic images.

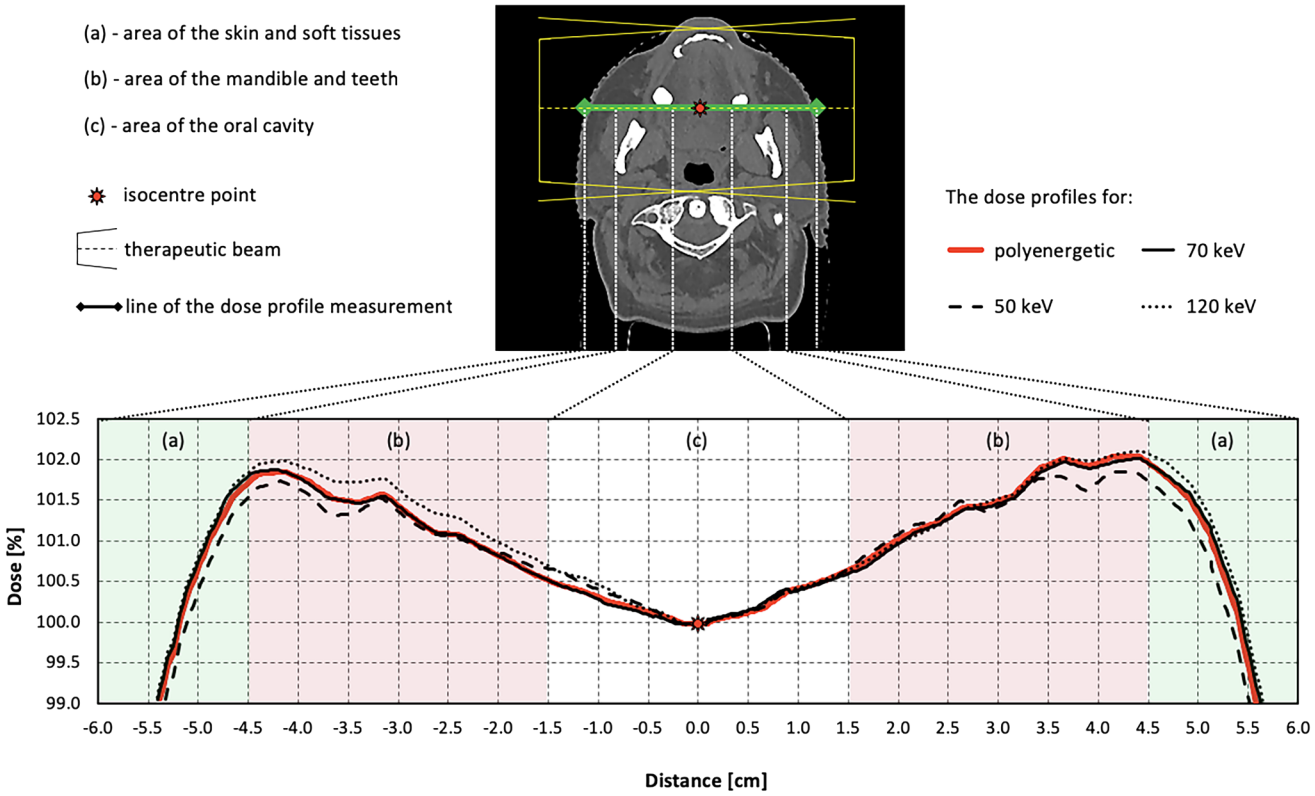

Fig. 6. The differences between doses calculated on four different sets of images (i.e. three sets of monoenergetic images with energies of 50 keV, 70 keV, 120 keV and one set of polyenergetic images) while one calibration curve (for polyenergetic images) was applied.

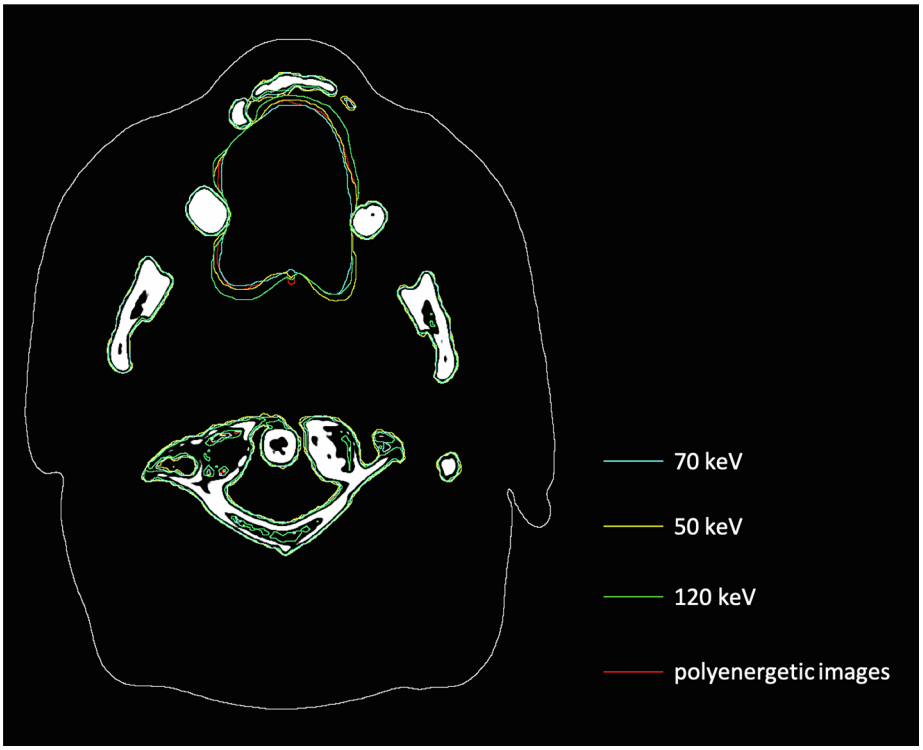

Fig. 7. The outlines for the bones (automatic segmentation) and for the tongue (manual segmentation) prepared on four different sets of images, i.e. on three monoenergetic sets with energies of 50 keV, 70 keV and 120 keV and on one set of polyenergetic images.

Table 2
The differences between the outlines obtained from set of 70 keV images and the outlines from the sets of 50 keV, 120 keV and polyenergetic images.

Structure:	Bones		Tongue	
Method of segmentation:	Automatic		Manual	
Reference outlines: 70 keV	DSC	V_{norm} [%]	DSC	V_{norm} [%]
50 keV:	1.000	109.1	0.994	117.0
120 keV:	0.940	89.0	0.995	131.7
polyenergetic images:	0.976	99.8	0.996	101.7

DSC – Sørensen–Dice coefficient between the structure contoured on X set of images and the same structure contoured on the set of images with energy of 70 keV.
V_{norm} [%] – Volume of the structure contoured on X set of images, normalised to volume of the same structure contoured on the set of images with energy of 70 keV.

5. Conclusion

To improve relative uniformity, low contrast resolution, noise and signal to noise ratio, monoenergetic CT sets of images reconstructed from dual energy CT scanning can be used. The best results of the above pointed parameters were obtained for images reconstructed for energy of 70 keV that are potentially the best for radiotherapy treatment plan preparation.

Declaration of Competing Interest

None.

Acknowledgements

This study was supported by the Greater Poland Cancer Centre institutional grant no 19/2015(111).

References

[1] McCollough CH, Leng S, Yu L, Fletcher JG. Dual- and multi-energy CT: principles, technical approaches, and clinical applications. Radiology 2015;276(3):637–53.
[2] Zarzour JG, Milner D, Valentin R, Jackson BE, Gordetsky J, West J, et al. Quantitative iodine content threshold for discrimination of renal cell carcinomas using rapid kV-switching dual-energy CT. Abdom Radiol (NY) 2017;42(3):727–34.
[3] Flohr TG, McCollough CH, Bruder H, Petersilka M, Gruber K, Süss C, et al. First performance evaluation of a dual-source CT (DSCT) system. Eur Radiol 2006;16(2):256–68.
[4] Johnson TR, Krauss B, Sedlmair M, Grasruck M, Bruder H, Morhard D, et al. Material differentiation by dual energy CT: initial experience. Eur Radiol 2007;17(6):1510–7.
[5] Matsubara K, Nagata H, Okubo R, Takata T, Kobayashi M. Method for determining the half-value layer in computed tomography scans using a real-time dosimeter: application to dual-source dual-energy acquisition. Phys Med 2017;44:227–31.
[6] Kalender WA, Klotz E, Suess C. Vertebral bone mineral analysis: an integrated approach with CT. Radiology 1987;164(2):419–23.
[7] Kalender WA, Perman WH, Vetter JR, Klotz E. Evaluation of a prototype dual energy computed tomographic apparatus. I. Phantom studies. Med Phys 1986;13(3):334–9.
[8] Patel BN, Marin D. Strategies to improve image quality on dual-energy computed tomography. Radiol Clin North Am 2018;56(4):641–7.
[9] Alvarez RE, Macovski A. Energy-selective reconstructions in x-ray computerized tomography. Phys Med Biol 1976;21(5):733–44.
[10] Macovski A, Alvarez RE, Chan JL, Stonestrom JP, Zatz LM. Energy dependent reconstruction in x-ray computerized tomography. Comput Biol Med 1976;6(4):325–36.
[11] Tsang DS, Merchant TE, Merchant SE, Smith H, Yagil Y, Hua C-H. Quantifying potential reduction in contrast dose with monoenergetic images synthesized from dual-layer detector spectral CT. Br J Radiol 2017;90:20170290.
[12] Mei K, Ehn S, Oechsner M, Kopp FK, Pfeiffer D, Fingerle AA, et al. Dual-layer spectral computed tomography: measuring relative electron density. Eur Radiol Exp 2018;2:20.
[13] Sakabe D, Funama Y, Taguchi K, Nakaura T, Utsunomiya D, Oda S, et al. Image quality characteristics for virtual monoenergetic images using dual-layer spectral detector CT: comparison with conventional tube-voltage images. Phys Med 2018;49:5–10.
[14] van Ommen F, Bennink E, Vlassenbroek A, Dankbaar JW, Schilham AMR, Viergever MA, et al. Image quality of conventional images of dual-layer SPECTRAL CT: a phantom study. Med Phys 2018;45(7):3031–42.
[15] Shikhaliev PM. Energy-resolved computed tomography: first experimental results. Phys Med Biol 2008;53(20):5595–613.
[16] Taguchi K, Iwanczyk JS. Vision 20/20: single photon counting X-ray detectors in medical imaging. Med Phys 2013;40(10):100901.
[17] Atak H, Shikhaliev PM. Dual energy CT with photon counting and dual source systems: comparative evaluation. Phys Med Biol 2015;60(23):8949–75.
[18] Leng S, Zhou W, Yu Z, Halaweish A, Krauss B, Schmidt B, et al. Spectral performance of a whole-body research photon counting detector CT: quantitative accuracy in derived image sets. Phys Med Biol 2017;62(17):7216–32.
[19] Gulliksrud K, Stokke C, Martinsen AC. How to measure CT image quality: variations in CT-numbers, uniformity and low contrast resolution for a CT quality assurance phantom. Phys Med 2014;30(4):521–6.
[20] Verdun FR, Racine D, Ott JG, Tapiovaara MJ, Toroi P, Bochuda FO, et al. Image quality in CT: from physical measurements to model observers. Phys Med 2015;31(8):823–43.
[21] ARTISCAN Details of parameters, Phantom CATPHAN Modality CT, Annex A1.27. http://www.aquilab.com.
[22] Catphan 500 and 600 Manual. The Phantom Laboratory. https://www.phantomlab.com.
[23] Sørensen T. A method of establishing groups of equal amplitude in plant sociology based on similarity of species and its application to analyses of the vegetation on Danish commons. Kongelige Danske Videnskabernes Selskab 1948;5(4):1–34.
[24] Dice LR. Measures of the amount of ecologic association between species. Ecology 1945;26(3):297–302.